Response of mechanically strained nanomaterials to irradiation: Insight from atomistic simulations

E. Holmström,[1] L. Toikka,[1] A. V. Krasheninnikov,[1,2] and K. Nordlund[1]
[1]*Materials Physics Division and Helsinki Institute of Physics, University of Helsinki, P.O. Box 43, FI-00014 Helsinki, Finland*
[2]*Department of Applied Physics, Aalto University, P.O. Box 1100, FI-00076 AALTO, Finland*
(Received 10 May 2010; revised manuscript received 2 July 2010; published 20 July 2010)

By combining analytical molecular-dynamics with density-functional theory simulations, we study the radiation hardness of *mechanically strained* low-dimensional nanosystems such as carbon nanotubes, graphene, and Si nanowires. We show that the radiation hardness of all these structures decreases with strain but the effect is most pronounced in nanowire due to the bulk structure of its core in contrast with the planar structure of nanotubes and graphene. Our results not only elucidate the microscopic mechanism of irradiation-induced defect production in strained nanomaterials but also provide quantitative information required for assessing the stability of nanocomponents in composite materials subjected to mechanical strain and irradiation, e.g., in space applications.

DOI: 10.1103/PhysRevB.82.045420 PACS number(s): 61.80.Az, 61.72.Bb, 81.07.De

I. INTRODUCTION

The intriguing behavior of various nanomaterials subjected to electron[1–4] and ion[5–7] irradiation has stimulated a considerable body of research aimed at not only understanding irradiation effects in nanoscale systems but also at exploring the possibility of using particle beams as a tool to tailor system properties.[8,9] It has been shown, in particular, that irradiation can improve the mechanical properties of multiwalled nanotubes,[2,10] bundles of single-walled nanotubes (SWNTs),[4] and even nanotube mats and fibers.[11,12] The explanation for this observation is irradiation-induced cross linking between nanotubes which individually exhibit outstanding mechanical characteristics but are normally loosely connected.

In all previous experimental studies, the system was irradiated first, and only then mechanical properties were measured. However, there is very little fundamental knowledge of how mechanically strained nanomaterials respond to ion or electron bombardment. At the same time, this issue is not only of academic, but also of high practical interest. In a radiation-rich environment, the mechanical and electronic properties of nanomaterials may deteriorate faster when strain is present, especially when the strain approaches the elastic limit. Such a situation might be realized in space applications, e.g., in the trunk of the widely discussed space elevator,[13] which if created, will be subject to considerable strain and open space irradiation. The possibility of tuning the band structure of semiconductor nanowires (NWs) by strain[14,15] and their application in transistor and solar-cell technology[16] also calls for understanding their response to irradiation under strain. Moreover, strained SiGe semiconductor nanostructures are already industrially used to speed up the operation of metal-oxide-semiconductor field-effect transistor transistors.[17]

In this study we use quantum-mechanical and classical molecular-dynamics (MDs) computer simulations to study the response of mechanically strained nanomaterials to irradiation. We concentrate on two representative systems: single-walled carbon nanotubes and Si NWs. By calculating the threshold displacement energy, the single most important parameter which describes the response of a material to irradiation, as a function of mechanical strain, we demonstrate that the effect of strain on radiation hardness is much more severe for Si NWs than for SWNTs. Moreover, in the case of nanotubes, small strain can surprisingly increase their stability under irradiation. We show that such a behavior originates from a different atomic structure ("tubular" vs "bulk" geometry) of these nanosystems.

II. SINGLE-WALLED CARBON NANOTUBES

The reason for choosing SWNTs and Si NWs is that their atomic structures are typical for many other nanomaterials: while the SWNT represents an atom-thick tubular system, the Si NW has essentially the structure of bulk Si, but with nanoscale dimensions. Both materials display excellent mechanical properties and a number of reports on their striking behavior under irradiation have recently appeared.[2,3,5]

To assess the response of mechanically strained nanomaterials to irradiation, we concentrate on calculations of the displacement threshold energy T_d as a function of strain. Being a critical input parameter in the Kinchin-Pease[18] and other semiclassical theories of defect production and ion stopping,[19] T_d is a crucial characteristic describing the radiation hardness of a material. For SWNTs and the surface of the Si NW, we define T_d as the minimum kinetic energy required to take the recoil atom to infinity by sputtering. For the bulk core of the Si NW, we define T_d^{FP} as the recoil energy required to create a stable vacancy-interstitial (Frenkel) pair in the crystal structure.

To understand the effect of strain ϵ on T_d in SWNTs, we employed MD with the nonorthogonal density-functional-based tight-binding (DFTB) force model[20] for describing the interaction of C atoms at the quantum-mechanical level. The simulations were carried out in a similar manner as in previous works[21,22] that showed good agreement with experiments regarding the dependence of the threshold displacement energy on the size of the nanotube.[23] Simulations were carried out for armchair and zigzag SWNTs with diameters of 6 to

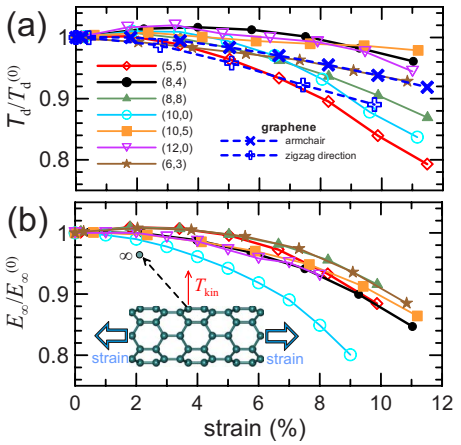

FIG. 1. (Color online) (a) Displacement threshold energy T_d as a function of strain calculated dynamically using DFTB molecular dynamics in nanotubes with various chiralities and in graphene. T_d is normalized to the value of $T_d^{s,(0)}$ at zero strain. (b) Energy E_∞ required to take a C atom to infinity as a function of strain calculated statically using the DFTB model for the same nanotubes. The inset shows the simulation setup used.

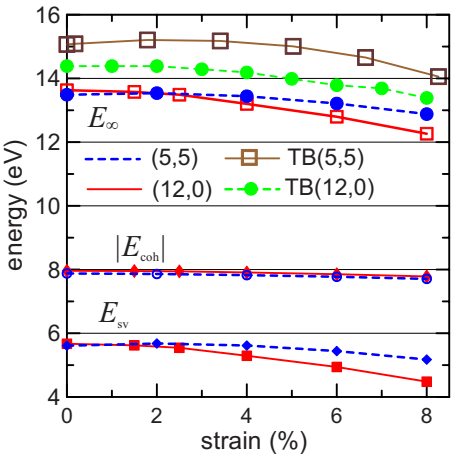

FIG. 2. (Color online) Energy E_∞ required to take a C atom to infinity from (5,5) and (10,0) nanotubes as a function of strain as calculated by the plane-wave DFT code VASP and DFTB. The DFT results for the cohesive energy E_{coh} and single vacancy formation energy E_{SV} are also shown.

17 Å and lengths of 12–23 Å. Periodic boundary conditions along the tube axis were used. The atom positions were fully optimized for every strain value. After assigning the initial kinetic energy to one of the atoms, free MD was run for 1 ps. The recoil momentum vector was perpendicular to the SWNT surface, as such a configuration corresponds to the smallest escape energy.[22] The absolute values of T_d were in the range of 17–21 eV in agreement with previous calculations.[21,22]

Figure 1(a) shows T_d as a function of ϵ for SWNTs with various chiralities. To facilitate the comparison of the results for different tubes, T_d was normalized over the displacement threshold energy for the unstrained system, $T_d^{(0)}$. It is evident that although the results depend on the tube chirality, for all the SWNTs studied, T_d insignificantly (less than 4%) decreases for ϵ up to 5%. An ϵ of ~10% brings a more notable drop in T_d of about 5–15 %. We also carried out simulations for zigzag and armchair graphene ribbons with qualitatively similar results. Such a general behavior can be expected, as strain weakens C-C bonds, so that less energy is required for bond rupture. Surprisingly for some nanotubes, however, a small strain gives rise to an *increase* in T_d.

To understand the origin of this effect, which may arise from strain-related changes in the potential barrier for atomic displacement or from energetics of the strained tube, we also calculated statically the energy E_∞ required to take a C atom to infinity,

$$E_\infty = E(N-1) + E(1) - E(N), \tag{1}$$

where $E(1)$ is the energy of an isolated C atom, $E(N-1)$ is the total energy of the system with a single vacancy, and $E(N)$ is the energy of the pristine system composed of N atoms. The static DFTB simulations gave qualitatively similar results as the dynamical simulations, Fig. 1(b), indicating that the increase in T_d for small values of ϵ is associated mostly with the energetics of defects, although dynamic effects such as changes in the recoil direction corresponding to the minimum escape energy may also contribute.

As the DFTB approach makes use of a considerable number of approximations, we also calculated E_∞ within the framework of rigorous density-functional theory (DFT) as implemented in the plane-wave (PW) basis-set VASP (Ref. 24) code. We used projector augmented wave potentials[25] to describe the core electrons and the generalized gradient approximation[26] for exchange and correlation. A kinetic-energy cutoff of 400 eV was used. Increasing the cutoff energy up to 600 eV changed the bonding energies by less than 10 meV. The same accuracy was also achieved with respect to the **k**-point sampling over the Brillouin zone (with meshes up to 15 **k** points along the tube axis). This approach has been demonstrated to be adequate for the modeling of defects in graphitic systems.[27,28] Figure 2 shows E_∞ as a function of ϵ for the (5,5) and (12,0) SWNTs. The PW-DFT and DFTB results are in qualitative agreement, although the PW-DFT approach gives a smaller increase in E_∞. Thus, the unexpected enhancement of T_d and E_∞, which can be associated with a higher radiation tolerance, is not an artifact of the DFTB approach or our simulation setup used in the dynamical calculations.

We note that Eq. (1) can be rewritten in terms of the well-defined physical quantities of cohesive energy E_{coh} and single-vacancy (SV) formation energy E_{SV}, as

$$E_\infty = |E_{coh}| + |E_{SV}|, \tag{2}$$

where the energies are defined, as usual, as

$$E_{coh} = E(N)/N - E(1), \tag{3}$$

$$E_{SV} = E(N-1) + E(N)/N - E(N). \tag{4}$$

As E_{SV} is positively defined, while E_{coh} is negative, absolute values are used in Eq. (2) to make the analysis more transparent.

E_{coh} and E_{SV} are presented in Fig. 2 for the (5,5) and (12,0) SWNTs. As expected, E_{coh} monotonically drops with ϵ as all the bonds are weakened. E_{SV} slightly increases at $\epsilon > 2\%$, then drops. To understand this effect, one should recall that the SV in graphene and SWNTs reconstructs[29] by forming a new bond oriented perpendicular to the tube axis. This gives rise to a local contraction of the SWNT diameter, and, due to the elasticity of the carbon network, to a minor expansion along the axis.[29] Small increase in the SWNT length at small ϵ gives rise to a counter effect of bond weakening. Depending on chirality, the bonds can be oriented in different ways in the SWNT, so the interplay between E_{coh} and E_{SV} can give rise to different net effects at small strain, whereas for large values of ϵ the effect of bond weakening dominates.

As the changes in T_d are less than 4% for ϵ up to 5%, one can expect that strain will not have a strong effect on the radiation tolerance of nanotube-based materials at small values of ϵ. However, at higher strains of $\epsilon > 10\%$ the effect may be noticeable. For example, considering the radiation spectrum of low-energy (up to 300 keV) protons at geosynchronous orbit,[30] a drop of $\sim 15\%$ in T_d results in an increase of 30% in the damage rate in SWNTs according to a SRIM (Ref. 31) calculation. For 500 keV electrons, the corresponding increase in damage production is also 30%, as estimated within the McKinley-Feshbach formalism.[32]

III. SILICON NANOWIRE

Having assessed the effects of strain on the response of SWNTs to irradiation, we moved on to Si NWs. Previous quantum-mechanical DFT (Refs. 33 and 34) and TB (Refs. 35 and 36) studies of threshold defect production in silicon have focused on bulk systems with a relatively small number of atoms (about 100), as such methods are prohibitively expensive for large systems. Hence, as the number of atoms in a NW with any realistic diameter is considerably larger than in SWNTs, we could not use the DFT approach (even by using the sudden approximation approach[33]), and the NW was modeled using the well-established Stillinger-Weber analytical potential instead.[37] We have recently shown that out of commonly used classical potentials, Stillinger-Weber gives threshold energies overall closest to DFT calculations.[34] An illustration of the wire is shown in Fig. 3(a). The system was 103 Å in length and 43 Å in diameter with a hexagonal cross section. The NW axis coincided with the $\langle 111 \rangle$ direction and the $2 \times (7.68)$ surface reconstruction[38] was taken into account. This has been found to be the most stable type of small-diameter Si nanowire.[39] The reconstructed [112] face of the wire comprises six sublattices of equivalent sites, labeled from A to F as illustrated in Fig. 3(b).

First, we performed static calculations of the formation energies of low-energy point defects. We considered the SV at the surface of the wire at each of the six atomic sites. In the core of the wire, the SV, interstitial-vacancy (Frenkel) pair, and the fourfold coordinated bond defect[40,41] were studied. Next, dynamical simulations were performed for investigating T_d^{FP} in the wire core and T_d at the surface. At each

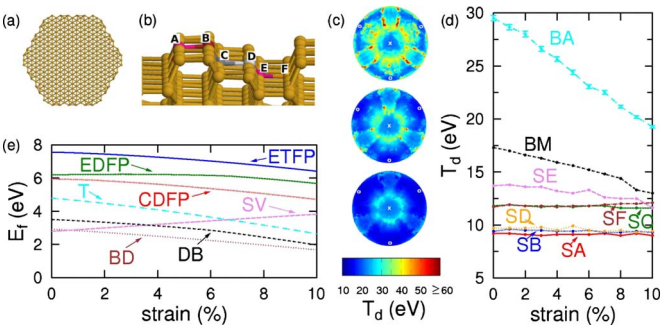

FIG. 3. (Color online) (a) Cross section of the studied nanowire. (b) The six nonequivalent atomic sites on the surface of the wire. (c) Visualization of the threshold energy surface for an atom in the core of the wire at strains of ϵ=0%, 5%, and 10% from top down. The closed $\langle 111 \rangle$ direction is marked by "x" and the open direction by "o." (d) Results from the dynamical simulations: average threshold displacement energy in the bulk core (BA), minimum threshold energy in the core (BM), and minimum sputtering threshold energy for each atom on the surface (SA, SB, SC, SD, SE, and SF). (e) Formation energies of various defects in the core of the wire: tetrahedral interstitial (T), dumbbell or split interstitial (DB), SV, bond defect (BD), extended Frenkel pair with a dumbbell interstitial (EDFP), the same with a tetrahedral interstitial (ETFP), and a close Frenkel pair with a dumbbell interstitial (CDFP).

value of ϵ, T_d^{FP} in the core of the wire was determined in 1000 randomly chosen directions, and in addition to the global minimum of T_d^{FP} over all directions, the average of T_d^{FP} was calculated as the arithmetic mean over the threshold energies. Then, T_d for each of the six sites on the surface was determined.

The formation energies of defects in the core of the wire are presented in Fig. 3(e) as functions of ϵ. The general theory of the effect of stress on the formation energy of a given defect is well established in the literature.[42,43] In the core of the nanowire, the formation energy of the single vacancy was found to nearly perfectly follow the theoretical prediction,

$$E_f(p) = E_f(p=0) + pV_f, \tag{5}$$

where E_f is the formation energy of the defect, p is the total pressure, and V_f is the formation volume (formation volume tensor in the general case). Note that positive values of strain correspond to negative values of p in Eq. (5). From this, we deduce that the behavior of the formation energies of the studied point defects in the core of the wire is practically identical to their behavior in regular bulk silicon, assuming positive V_f for interstitial-type defects and negative V_f for vacancies. The most important observation here in terms of threshold defect production is that the formation energy of the Frenkel pair decreases with ϵ, except for a slight initial increase in the case of the extended Frenkel pair including a dumbbell interstitial. On the surface of the wire, the formation energy of the vacancy displayed little change as the wire was stretched. This is because the bonds around the atoms around a surface vacancy can rearrange to reduce the net effect of strain on the defect formation energy.

The results of the dynamical simulations are presented in Figs. 3(c) and 3(d). In Fig. 3(d), both the average and minimum of T_d^{FP} are seen to decrease linearly as the wire is strained. These general observations can be explained by two factors. First, as the wire is stretched to $\epsilon=10\%$, the volume per atom ratio in the core increases linearly from ~20 to 21 Å^3, which makes it easier for an atom to settle into an interstitial position. Second, as the wire is stretched, the bonds in the ⟨111⟩ direction in particular are also stretched while the other three bonds of each atom are twisted out of their optimal orientations. This makes the bonds weaker, which is seen as an increase in the potential energy of an atom in the core by ~0.1 eV as ϵ approaches 10%. Now, the process of creating a Frenkel pair through an atomic recoil involves the breaking and twisting of a number of bonds in the region surrounding the recoil. Hence in the strained wire, the combination of weaker bonds and a larger volume per atom ratio makes it is easier for an atom to pave its way through the lattice and to settle into an interstitial site. From the visualization of the threshold energy surface in Fig. 3(c) it is seen that as the wire is strained, the maxima in T_d^{FP} are quickly smeared out, and at $\epsilon=10\%$ the surface is remarkably isotropic. Finally, as was the case with the SWNTs, we note a qualitative correlation between the behavior of the dynamical results for T_d and the corresponding defect energetics as a function of strain.

For the surface of the wire, T_d is presented in Fig. 3(d) for each atom type. It is seen that T_d remains nearly constant for atoms A, B, C, and D. This is because changes in the bond strengths of the surface atoms are very small. However, as the wire is strained, the surface structure relaxes in such a way that atoms E and F have a more direct route for sputtering, and thus they are less prone to being slowed down by atoms nearby them. This effect is partly compensated, however, for atom F by the nearby atom A, so that T_d stays nearly constant as the wire is strained. Note also the correlation of these dynamic results to the nearly constant formation energies of surface vacancies.

Armed with the knowledge of the effect of ϵ on T_d, we can estimate the effect of strain on damage production for Si NW. Considering again the proton spectrum at a geosynchronous orbit, SRIM predicts that the damage production rate increases by 30% in the core of the wire for already $\epsilon=5\%$ and as much as 80% in the bulk core of the wire for $\epsilon=10\%$. For 500 keV electrons the increase is 100% and 300%, respectively. The much lower albeit constant threshold energy of the surface atoms implies a high and constant defect production rate there, but the larger the diameter of the wire, the more significant the increase in defect production in the bulk core is.

IV. DISCUSSION AND CONCLUSIONS

The comparison of the response to irradiation of mechanically strained carbon SWNTs and Si NWs indicates that although the radiation tolerance of either material decreases with strain as the stretched bonds become weaker, the effect is much stronger in NWs. This is associated with the difference in the atomic structure of these materials: while nanotubes consist of essentially "surface" atoms, Si NWs have the structure of bulk Si, but with nanoscale dimensions. As the production of defects in bulk material is governed by the availability of open space for interstitials which increases with strain, the radiation tolerance of the NWs quickly decreases with strain. One can assume that our results should be relevant to other systems with similar structure. Thus our results set the limit on strain values beyond which the effects of strain should be taken into account when estimating the radiation tolerance of not only SWNTs and Si NWs in radiation-rich environments, e.g., open space applications, but also in other nanomaterials.

In conclusion, using classical and quantum-mechanical molecular-dynamics simulations, we studied the radiation response of mechanically strained low-dimensional nanostructures. In general, the radiation hardness of SWNTs and Si NWs was found to decrease with increasing strain, but the effect is much stronger in Si NWs due to its bulklike atomic structure in contrast to the tubular structure of SWNT, a result which we believe can be extrapolated to a wide variety of nanosystems with similar atomic structures. Curiously, SWNTs with certain chiralities display a slight increase in the threshold displacement energy for small values of strain, which can be attributed to the reconstruction of the single vacancy. Additionally, the behavior of the threshold displacement energy was found to correlate qualitatively with the relevant defect formation energies in both SWNTs and Si NWs. Our results elucidate the microscopic mechanism of irradiation-induced defect production in strained nanomaterials and provide quantitative information required for assessing the stability of nanocomponents in composite materials subjected to mechanical strain and irradiation, e.g., in open space applications.

ACKNOWLEDGMENTS

We thank the Finnish IT Center for Science for generous grants of computer time. This work was supported by the Academy of Finland through several projects and the Centre of Excellence program.

[1] J. H. Warner, M. H. Rümmeli, L. Ge, T. Gemming, B. Montanari, N. M. Harrison, B. Büchner, and G. Briggs, Nat. Nanotechnol. **4**, 500 (2009).

[2] B. Peng, M. Locascio, P. Zapol, S. Li, S. L. Mielke, G. C. Schatz, and H. D. Espinosa, Nat. Nanotechnol. **3**, 626 (2008).

[3] L. Sun, F. Banhart, A. V. Krasheninnikov, J. A. Rodríguez-Manzo, M. Terrones, and P. M. Ajayan, Science **312**, 1199 (2006).

[4] A. Kis, G. Csányi, J.-P. Salvetat, T.-N. Lee, E. Couteau, A. J. Kulik, W. Benoit, J. Brugger, and L. Fórro, Nature Mater. **3**, 153

(2004).
[5] A. Colli, A. Fasoli, C. Ronning, S. Pisana, S. Piscanec, and A. C. Ferrari, Nano Lett. **8**, 2188 (2008).
[6] B. Q. Wei, J. D'Arcy-Gall, P. M. Ajayan, and G. Ramanath, Appl. Phys. Lett. **83**, 3581 (2003).
[7] S. Talapatra, P. G. Ganesan, T. Kim, R. Vajtai, M. Huang, M. Shima, G. Ramanath, D. Srivastava, S. C. Deevi, and P. M. Ajayan, Phys. Rev. Lett. **95**, 097201 (2005).
[8] A. V. Krasheninnikov and F. Banhart, Nature Mater. **6**, 723 (2007).
[9] A. Krasheninnikov and K. Nordlund, J. Appl. Phys. **107**, 071301 (2010).
[10] E. M. Byrne, M. A. McCarthy, Z. Xia, and W. A. Curtin, Phys. Rev. Lett. **103**, 045502 (2009).
[11] J. A. Åström, A. V. Krasheninnikov, and K. Nordlund, Phys. Rev. Lett. **93**, 215503 (2004); **94**, 029902(E) (2005).
[12] V. Skákalová, A. B. Kaiser, Z. Osváth, G. Vértesy, L. P. Biró, and S. Roth, Appl. Phys. A: Mater. Sci. Process. **90**, 597 (2008).
[13] B. C. Edwards, Acta Astronaut. **47**, 735 (2000).
[14] A. J. Lu, R. Q. Zhang, and S. T. Lee, Appl. Phys. Lett. **92**, 203109 (2008).
[15] D. B. Migas and V. E. Borisenko, Nanotechnology **18**, 375703 (2007).
[16] W. Lu and C. M. Lieber, J. Phys. D **39**, R387 (2006).
[17] S. E. Thompson *et al.*, IEEE Trans. Electron Devices **51**, 1790 (2004).
[18] G. Kinchin and R. Pease, Rep. Prog. Phys. **18**, 1 (1955).
[19] J. F. Ziegler, J. P. Biersack, and U. Littmark, *The Stopping and Range of Ions in Matter* (Pergamon, New York, 1985).
[20] T. Frauenheim, G. Seifert, M. Elstner, T. Niehaus, C. Köhler, M. Amkreutz, M. Sternberg, Z. Hajnal, A. Di Carlo, and S. Suhai, J. Phys.: Condens. Matter **14**, 3015 (2002).
[21] A. V. Krasheninnikov, F. Banhart, J. X. Li, A. S. Foster, and R. M. Nieminen, Phys. Rev. B **72**, 125428 (2005).
[22] A. Zobelli, A. Gloter, C. P. Ewels, G. Seifert, and C. Colliex, Phys. Rev. B **75**, 245402 (2007).
[23] J. H. Warner, F. Schäffel, G. Zhong, M. H. Rümmeli, B. Büchner, J. Robertson, and G. Briggs, ACS Nano **3**, 1557 (2009).
[24] G. Kresse and J. Furthmüller, Comput. Mater. Sci. **6**, 15 (1996).
[25] P. E. Blöchl, Phys. Rev. B **50**, 17953 (1994).
[26] J. P. Perdew, J. A. Chevary, S. H. Vosko, K. A. Jackson, M. R. Pederson, D. J. Singh, and C. Fiolhais, Phys. Rev. B **46**, 6671 (1992).
[27] P. O. Lehtinen, A. S. Foster, Y. Ma, A. V. Krasheninnikov, and R. M. Nieminen, Phys. Rev. Lett. **93**, 187202 (2004).
[28] A. V. Krasheninnikov, P. O. Lehtinen, A. S. Foster, P. Pyykkö, and R. M. Nieminen, Phys. Rev. Lett. **102**, 126807 (2009).
[29] A. V. Krasheninnikov, P. O. Lehtinen, A. S. Foster, and R. M. Nieminen, Chem. Phys. Lett. **418**, 132 (2006).
[30] D. Scott and D. Marvin, Conference Record of the 23rd IEEE Photovoltaic Specialists Conference, p. 1338 (1993).
[31] J. F. Ziegler, SRIM-2008 software package, available online at http://www.srim.org
[32] F. Banhart, Rep. Prog. Phys. **62**, 1181 (1999).
[33] W. Windl, T. J. Lenosky, J. D. Kress, and A. F. Voter, Nucl. Instrum. Methods Phys. Res. B **141**, 61 (1998).
[34] E. Holmström, A. Kuronen, and K. Nordlund, Phys. Rev. B **78**, 045202 (2008).
[35] S. Uhlmann, T. Frauenheim, K. Boyd, D. Marton, and J. Rabalais, Radiat. Eff. Defects Solids **141**, 185 (1997).
[36] M. Mazzarolo, L. Colombo, G. Lulli, and E. Albertazzi, Phys. Rev. B **63**, 195207 (2001).
[37] F. H. Stillinger and T. A. Weber, Phys. Rev. B **31**, 5262 (1985).
[38] C. Fulk, S. Sivananthan, D. Zavitz, R. Singh, M. Trenary, Y. P. Chen, G. Brill, and N. Dhar, J. Electron. Mater. **35**, 1449 (2006).
[39] I. Ponomareva, M. Menon, D. Srivastava, and A. N. Andriotis, Phys. Rev. Lett. **95**, 265502 (2005).
[40] M. Tang, L. Colombo, J. Zhu, and T. Diaz de la Rubia, Phys. Rev. B **55**, 14279 (1997).
[41] S. Goedecker, T. Deutsch, and L. Billard, Phys. Rev. Lett. **88**, 235501 (2002).
[42] M. J. Aziz, Mater. Sci. Semicond. Process. **4**, 397 (2001).
[43] M. S. Daw, W. Windl, N. N. Carlson, M. Laudon, and M. P. Masquelier, Phys. Rev. B **64**, 045205 (2001).